polymers

MDPI

Article

Nanocomposite of Fullerenes and Natural Rubbers: MARTINI Force Field Molecular Dynamics Simulations

Jiramate Kitjanon [1,2], Wasinee Khuntawee [1,2,3], Saree Phongphanphanee [2,3,4], Thana Sutthibutpong [2,3,5], Nattaporn Chattham [1], Mikko Karttunen [6,7,8] and Jirasak Wong-ekkabut [1,2,3,*]

1 Department of Physics, Faculty of Science, Kasetsart University, Bangkok 10900, Thailand; k.jiramatez@gmail.com (J.K.); w.khuntawee@gmail.com (W.K.); nattaporn.c@ku.ac.th (N.C.)
2 Computational Biomodelling Laboratory for Agricultural Science and Technology (CBLAST), Faculty of Science, Kasetsart University, Bangkok 10900, Thailand; fscisrph@ku.ac.th (S.P.); thana.sut@kmutt.ac.th (T.S.)
3 Thailand Center of Excellence in Physics (ThEP Center), Commission on Higher Education, Bangkok 10400, Thailand
4 Department of Material Science, Faculty of Science, Kasetsart University, Bangkok 10900, Thailand
5 Department of Physics, Faculty of Science, King Mongkut's University of Technology Thonburi (KMUTT), Bangkok 10140, Thailand
6 Department of Chemistry, The University of Western Ontario, 1151 Richmond Street, London, ON N6A 3K7, Canada; mkarttu@uwo.ca
7 Department of Physics and Astronomy, The University of Western Ontario, 1151 Richmond Street, London, ON N6A 3K7, Canada
8 The Center for Advanced Materials and Biomaterials Research, The University of Western Ontario, London, ON N6A 3K7, Canada
* Correspondence: jirasak.w@ku.ac.th

check for updates

Citation: Kitjanon, J.; Khuntawee, W.; Phongphanphanee, S.; Sutthibutpong, T.; Chattham, N.; Karttunen, M.; Wong-ekkabut, J. Nanocomposite of Fullerenes and Natural Rubbers: MARTINI Force Field Molecular Dynamics Simulations. *Polymers* **2021**, *13*, 4044. https://doi.org/10.3390/polym13224044

Academic Editors: Riccardo Concu and Michael González-Durruthy

Received: 12 October 2021
Accepted: 16 November 2021
Published: 22 November 2021

Publisher's Note: MDPI stays neutral with regard to jurisdictional claims in published maps and institutional affiliations.

Abstract: The mechanical properties of natural rubber (NR) composites depend on many factors, including the filler loading, filler size, filler dispersion, and filler-rubber interfacial interactions. Thus, NR composites with nano-sized fillers have attracted a great deal of attention for improving properties such as stiffness, chemical resistance, and high wear resistance. Here, a coarse-grained (CG) model based on the MARTINI force field version 2.1 has been developed and deployed for simulations of *cis*-1,4-polyisoprene (*cis*-PI). The model shows qualitative and quantitative agreement with the experiments and atomistic simulations. Interestingly, only a 0.5% difference with respect to the experimental result of the glass transition temperature (T_g) of the *cis*-PI in the melts was observed. In addition, the mechanical and thermodynamical properties of the *cis*-PI-fullerene(C_{60}) composites were investigated. Coarse-grained molecular dynamics (MD) simulations of *cis*-PI-C_{60} composites with varying fullerene concentrations (0–32 parts per hundred of rubber; phr) were performed over 200 microseconds. The structural, mechanical, and thermal properties of the composites were determined. The density, bulk modulus, thermal expansion, heat capacity, and T_g of the NR composites were found to increase with increasing C_{60} concentration. The presence of C_{60} resulted in a slight increasing of the end-to-end distance and radius of the gyration of the *cis*-PI chains. The contribution of C_{60} and *cis*-PI interfacial interactions led to an enhancement of the bulk moduli of the composites. This model should be helpful in the investigations and design of effective fillers of NR-C_{60} composites for improving their properties.

Keywords: molecular dynamics simulations; natural rubber; *cis*-1,4-polyisoprene; MARTINI force field

1. Introduction

Natural rubber (NR), mainly consisting of *cis*-1,4polyisoprene (*cis*-PI) with high elasticity, is acknowledged to be virtually irreplaceable in applications such as tires and seals. However, the neat NR usually suffers from poor mechanical strength [1,2]. To alleviate this problem, reinforcing fillers are widely used to improve the mechanical properties

of NR materials. Impressive enhancements in the properties, including mechanical [3,4], optical [3,5,6], self-healing [7,8], electrical [4,6,9], thermal [4,6], rheological [4,9], and glass transition [10,11], have been reported. The mechanical properties of NR composites depend on many factors, such as the types, dimensions, concentrations, dispersion states, and alignments of the fillers [4,12,13].

Among the most important methods of tuning the properties of NR are the vulcanization and reinforcement by composites, in particular carbon black (CB) [14,15] Here, the focus is on the latter. The reinforcement of NR composites by carbon black (CB) has been intensively studied and broadly applied in truck and car tires [16,17]. CB may improve tensile properties [18], fatigue resistance [19], stiffness, and wear resistance [20]. The CB concentration has a significant influence on the rubber composite properties; e.g., increasing the amount of CB has been shown to lead to enhanced tear strength, tensile strength, and elastic modulus [21,22]. The study of Wang et al. [23] revealed that the piezoresistivity of CB-NR composites monotonically decreases with decreasing CB concentration. However, CB-reinforced nanocomposites at high loading have shown the decay of the storage modulus at high deformation, indicating high hysteresis [24,25]. This is called the Payne effect, and it has limited the application of CB-reinforced nanocomposites to tires. Moreover, CB is produced from petroleum feedstock, which has a negative impact on the environment [26].

NR composited with carbon-based nanoparticles, e.g., carbon nanotubes (CNT) or graphene, offers the possibility to produce lightweight composites with enhanced electrical and magnetic properties and thermal conductivity [4,27,28]. For example, it has been shown that a small amount of multiwalled carbon nanotubes (MWCNTs) at 0.5 parts per hundred (phr) in NR-MWCNTs composite could enhance the tensile strength, tensile modulus, and tear strength by 61%, 75%, and 59%, respectively [29]. Fullerene(C_{60}) has been extensively used as a filler in polymer composites, especially for poly(3-hexylthiophene) in polymer-based solar cells for low-cost power production [30–32], and, in combination with epoxy, it has been shown to result in enhancements in the mechanical properties, electrical conductivity, flame resistance, and anti-corrosion [33]. In addition, the presence of fullerenes in NR composites has been shown to increase the modulus at 100% (M_{100}), the modulus at 300% (M_{300}) of elongation, and the shore hardness [34]. It has also been reported that the addition of 0.75 phr of fullerene in NR increases the M_{100}, M_{200}, $M_{300,}$ and hardness by 178%, 137%, 113%, and 20.5%, respectively, compared to composites at 0.0065 phr of fullerene [35]. After aging (heating at 70° C for 168 h), Jurkowska et al. found an increase in the elastic modulus for [C_{60}] < 0.5 phr, and, interestingly, the elastic modulus decreased at [C_{60}] = 0.75 phr. That could substantially reduce the degradation effects of rubber composites [35].

Atomistic molecular dynamics (MD) simulations can provide nanoscale information, such as the dispersion and aggregation of fillers [36], segmental dynamics [37], polymer chain alignment [38], molecular interactions [36,37,39], and filler size effects [40]. Guseva et al. [37] investigated the macroscopic properties of non-crosslinked *cis*-PI films confined with silica substrate using atomistic MD simulations. Liu et al. [41] reported that the glass transition temperature (T_g) of the *cis*-PI film increased when the film thickness was decreased. They also reported that, compared to a pure polymer system, the T_g increased when the filler was added. Raffaini et al. [42] studied rubber–fullerene conformations and observed fullerene aggregation when rubber chains were modified with COOH-termination. Although atomistic MD has been widely used in investigations of reinforced polymer nanocomposites, such simulations are computationally expensive. To overcome this limitation, coarse-grained (CG) models have been developed to produce simplified representations of polymer molecules to access much larger time and length scales.

One of the earlier works on the simulations of polymer melts was the seminal paper by Kremer and Grest focusing on melts well above the glass transition temperature [43]. An important step toward coarse-graining was taken in the 1995 article of Forrest and Suter, who showed how softer pairwise interactions emerge from an atomistic model upon averaging over the pair distribution [44]. The following years were very active for

the development of CG models for polymers and polymer melts, including the works of Akkermans and Briels, who constructed a CG model with a focus on the preservation of thermodynamic properties [45], followed by a number of studies on the systematic coarse-graining of polymers and melts [46,47], modification of the dissipative particle dynamics (DPD) method for melts [48], and fluctuating soft-sphere models [49] with the aim of improving the accuracy of CG polymer melt modeling. Regarding the interactions of fullerenes and polymers, Huang et al. [50] developed a polymer-fullerene CG model for polymer-based solar cells, and Volgin et al. [51] investigated the diffusion of fullerenes using a CG model. Although there is no lack of CG models, the MARTINI force field [52,53] has become by far the most dominant one, and it has been used for simulations of amino acids, water, phospholipid membranes, fullerenes, some polymers, and RNA [54–61].

Recently, we introduced a MARTINI CG model for *cis*-PI to study natural rubber [62]. The interactions of the *cis*-PI and fullerene, however, were not included in the model. That is done in the current work by combining the CG models of *cis*-PI and fullerene to study *cis*-PI-C_{60} composites. The parameters are based on the MARTINI force field version 2.1 [52]. The thermodynamic and mechanical properties of the *cis*-PI-C_{60} composites were calculated and compered with the experiments and atomistic MD simulations. The influence of the C_{60} concentrations on the structural, mechanical, and thermal properties of the composites was analyzed. The results show that the interfacial interactions between the C_{60} and *cis*-PI play an essential role in the composites' mechanical properties.

2. Methodology

2.1. Molecular Dynamics Simulations

In this study, *cis*-PI in melts and *cis*-PI composites at different C_{60} concentrations were investigated by coarse-grained (CG) molecular dynamics (CGMD) simulations. The CG model for *cis*-PI was developed based on the MARTINI force field version 2.1 (University of Groninge, Groningen, The Netherlands) and is described in detail in Table S1. A coarse-grained or superatom bead was used to represent an isoprene monomer. CG mapping of stretching and bending parameters for the *cis*-PI beads from united-atom MD trajectories were published in our previous work [62]. All systems consisted of 500 chains of 32-mers *cis*-PI, which is equivalent to 16,000 CG beads in total (an isoprene monomer was mapped into one bead in the CG model).

C_{60} molecules were randomly placed into the *cis*-PI melts with the number of 53, 107, 213, and 427 molecules corresponding to concentrations of 4, 8, 16, and 32 parts per hundred of rubber (phr), respectively. The details of all simulations are shown in Table S2. The CG fullerene model for the C_{60} molecule called F16 was taken from Ref. [63]. After steepest descent energy minimization, CGMD simulations were performed using the GROMACS 5.1.1 (University of Groningen, Royal Institute of Technology, Groningen, The Netherlands) package [64]. The number of particles, temperature, and pressure were kept constant (NPT ensemble). *cis*-PI and C_{60} molecules were thermostatted separately at 300 K using the Parrinello-Donadio-Bussi velocity rescale algorithm with a time constant of 30 ps [65,66]. Pressure was held constant at 1 bar by the Parrinello-Rahman barostat [67] with a time constant of 1 ps and compressibility of 4.5×10^{-5} bar^{-1}. The reaction-field method was used for the long-range electrostatic interactions [68,69], Lennard-Jones interactions were cut off at 1.1 nm, and periodic boundary conditions were applied in all directions. The simulation protocol had been tested and used in several prior studies [38,70–73]. All production simulations were run with time step of 30 ps for 21 μs. To confirm that equilibration had been reached, time evolution for the end-to-end distance and the radius of gyration were calculated (see Figures S1 and S2). The last 5 μs were used for data analysis and errors were estimated using standard deviation (SD). Molecular visualizations were done using the Visual Molecular Dynamics (VMD) software (University of Illinois Urbana-Champaign, Urbana and Champaign, IL, USA) [74].

2.2. Calculation of Thermal and Mechanical Properties

Glass Transition Temperature (T_g)

The final states of the simulations after 21 μs were used as the initial structures to calculate the glass transition temperatures (T_g). The systems were cooled from 300 K to 100 K with 10 K interval. The cooling rate was 0.1 K.ns^{-1}. To equilibrate the systems, additional 500 ns were simulated at each temperature in the NPT ensemble. T_g was calculated using the intersection of the two lines describing the behavior at low and high temperatures on density-temperature (ρ-T) curves [75–77]. Density versus temperature curves for *cis*-PI in melts and composites are shown in Figure S3.

The thermal volume expansion coefficient (γ), specific heat capacity (c_p), and bulk modulus (κ) were calculated from the fluctuations of the simulation box volumes (V) and enthalpy (H) using:

$$\gamma = \frac{\langle VH \rangle - \langle V \rangle \langle H \rangle}{N_A k_B T^2 \langle V \rangle} \quad (1)$$

$$c_p = \frac{\left\langle (H - \langle H \rangle)^2 \right\rangle}{m N_A k_B T^2} \quad (2)$$

$$\kappa = \frac{k_B T \langle V \rangle}{\left\langle (V - \langle V \rangle)^2 \right\rangle} \quad (3)$$

where k_B is the Boltzmann constant, N_A Avogadro's number, and m is the total mass of the system in atomic mass units. The angular brackets refer to averaging over simulation time.

2.3. Calculation of Solvation Free Energy

Thermodynamic integration (TI) [78] was applied to calculate solvation free energies of C_{60} in water, pure *cis*-PI, and *cis*-PI-C_{60} composites. The last frame from each of the 21 μs simulations was used as the initial structure. A C_{60} was added into the system and used as a coupling molecule. After steepest descent energy minimization, the MD simulations with the coupling parameter (λ) between 0 and 1 with interval of 0.05 were performed under the NPT ensemble. All systems were run for 300 ns, and the last 100 ns was used for analysis. The Bennett acceptance ratio (BAR) was applied to estimate the solvation free energy [79]. The solvation free energies are shown in Table S3. The effect of C_{60} concentration is discussed in Section 3.4 (Figure 5).

3. Results and Discussion

3.1. Coarse-Grained Model Based on MARTINI Force Field of cis-1,4-Polyisoprene

The macroscopic and structural properties of the *cis*-PI in the melts were analyzed and compared to the experiments and atomistic simulations in order to validate the CG model (Table 1). The system density was found to be in good agreement, with the values being about 19% and 27% higher than in the experiments [80] and previous united-atom MD (UAMD) simulations [38], respectively. The thermal expansion coefficient was found to be 52% and 19% higher than in the experiments [81,82] and UAMD [38], respectively. In addition, the squared end-to-end distance (R_0), the squared radius of gyration (R_g), and polymer expansion factor ($< R_0^2 > / < R_g^2 >$) of the *cis*-PI in the melts are within 5% from the UAMD data [38]. R_0 is defined as the average distance between the first and the last CG bead of the *cis*-PI chain. R_g was computed using.

$$R_g^2 = \frac{1}{N} \sum_{i=1}^{N} (r_i - r_{cm})^2 \quad (4)$$

where r_i is the position of particle i and r_{cm} is the position of the center of mass of the cis-PI chain. However, the bulk modulus was 3.8-fold lower than in the experiments [83] and 2.6-fold below the previous UAMD simulations [38]. One of the major contributors to this decrease of bulk modulus is the reduction in the degrees of freedom upon coarse-graining

monomers into superatom beads, which diminishes the friction between branching atoms and changes entropy [84,85]. Higher mobility of the CG chains causes large fluctuations of the simulation box volume compared to the UAMD simulations [38].

Table 1. Macroscopic and structural properties of *cis*-PI in melts. R_0, R_g, and $< R_0^2 > / < R_g^2 >$ are the end-to-end distance, the radius of gyration, and polymer expansion factor, respectively.

Properties	Exp.	United Atom [38]	CG
Density; kg/m^3	910 [80]	853.9 ± 1.6	1087 ± 2.30
Bulk modulus; GPa	2.02 [83]	1.37 ± 0.02	0.53 ± 0.00
Thermal expansion; (10^{-4}/K)	6.1 [81,82]	7.80 ± 0.15	9.25 ± 0.02
$< R_0^2 >$	-	12.85 ± 0.41	13.28 ± 0.06
$< R_g^2 >$	-	2.07 ± 0.04	2.17 ± 0.01
$< R_0^2 > / < R_g^2 >$	-	6.20	6.11

3.2. Effect of C_{60} Concentration on Macroscopic and Structural Properties of cis-PI Composites

Adding C_{60} into the *cis*-PI composites leads to a linear increase in density (Figure 1a) due to the mass of the C_{60} filler. Figure 1b shows the enhancement of the bulk modulus as a function of the C_{60} concentration. A slow increase was found for [C_{60}] < 16 phr (2.17×10^{-4} GPa per 1 phr), followed by a rapid increase at [C_{60}] = 32 phr (4.81×10^{-4} GPa per 1 phr). The increases in the density and bulk moduli as a function of the C_{60} concentration is similar to previous UA simulations [86]. In addition, the thermal expansion coefficient (γ) and specific heat capacity (c_p) at 300 K were computed using Equations (1) and (2). In the composites, both quantities increased when the amount of C_{60} increased (Figure 1c,d), similar to what has been observed in previous MD [87] and experimental studies [88] of polymer carbon-based nanocomposites.

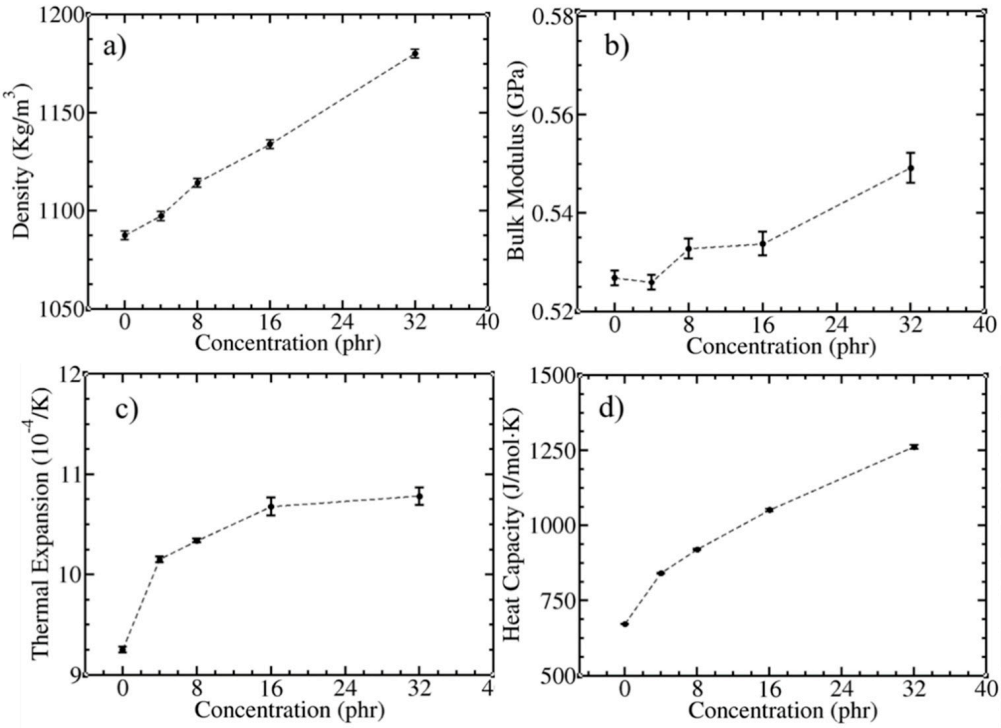

Figure 1. (**a**) Density, (**b**) bulk modulus (Equation (3)), (**c**) thermal expansion (Equation (1)), and (**d**) heat capacity (Equation (2)) of *cis*-PI and C_{60} composites as a function of C_{60} concentration.

The structural changes of the *cis*-PI chains at different C_{60} concentrations were also investigated by monitoring the R_0 and R_g. The averages of the R_0 and R_g for the last 5 μs

are provided in Table 2. For the *cis*-PI chains, they increased slightly upon increasing the amount of C_{60}. The polymer chain expansion factor ($< R_0{}^2 > / < R_g{}^2 >$) of the *cis*-PI in the melts was 6.11, which is in good agreement with previous UAMD simulations (6.20 [38] and 5.44 [77]) and refers to a random coil structure of a *cis*-PI chain [89].

Table 2. Average end-to-end distance (R_0), radius of gyration (R_g) of *cis*-PI chains, and their polymer chain expansion factor ($< R_0^2 > / < R_g^2 >$) as a function of C_{60} concentration.

C_{60} Concentration (phr)	$< R_0 >$ (nm)	$< R_g >$ (nm)	$< R_0^2 > / < R_g^2 >$
0	3.64 ± 0.06	1.47 ± 0.01	6.11
4	3.65 ± 0.06	1.48 ± 0.01	6.11
8	3.66 ± 0.06	1.48 ± 0.01	6.12
16	3.67 ± 0.06	1.48 ± 0.01	6.12
32	3.71 ± 0.06	1.50 ± 0.01	6.15

3.3. Effect of C_{60} Concentration on Microscopic Properties of cis-PI Composites

3.3.1. Interaction of C_{60}-C_{60} and C_{60}-*cis*-PI

To investigate the interaction free energy of C_{60}-C_{60} and C_{60}-*cis*-PI in the composites at different C_{60} concentrations, the potential of mean force (PMF) was calculated from the radial distribution function (RDF; $g(r)$) [90,91] as:

$$\mathrm{PMF} = -k_B T \ln(g(r)) \quad (5)$$

where k_B is the Boltzmann constant and T is the absolute temperature.

The dimerization free energies of C_{60} in *cis*-PI composites at different C_{60} concentrations are shown in Figure 2a. The first, second, and third minima of the C_{60}-C_{60} PMF corresponding to the distances between the neighboring C_{60} molecules are at 1.0 nm, 1.5 nm, and 1.9 nm, respectively. The second minimum is at the lowest free energy, suggesting energetic preference of C_{60} dimerization with the *cis*-PI chain insertion. That the polymer chains fill the space between the C_{60} molecules has also been observed in previous studies [38,59,60,92]. The PMF for C_{60} and *cis*-PI interactions is shown in Figure 2b. This result demonstrates the C_{60}-*cis*-PI composites' preference to a dispersed structure corresponding to the snapshots in (Figure 3), which show the dispersed structure for all the C_{60} concentrations.

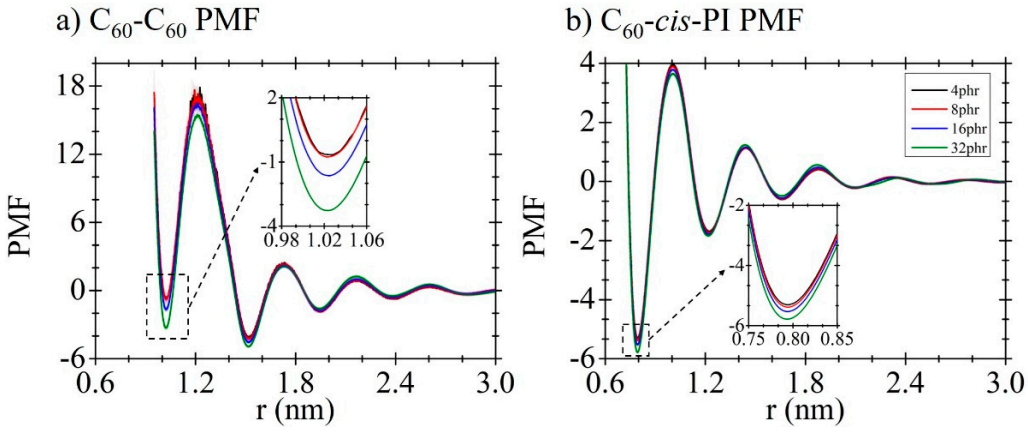

Figure 2. Potential of mean force (PMF) of (**a**) C_{60}-C_{60} and (**b**) C_{60}-*cis*-PI in the composites at different C_{60} concentrations.

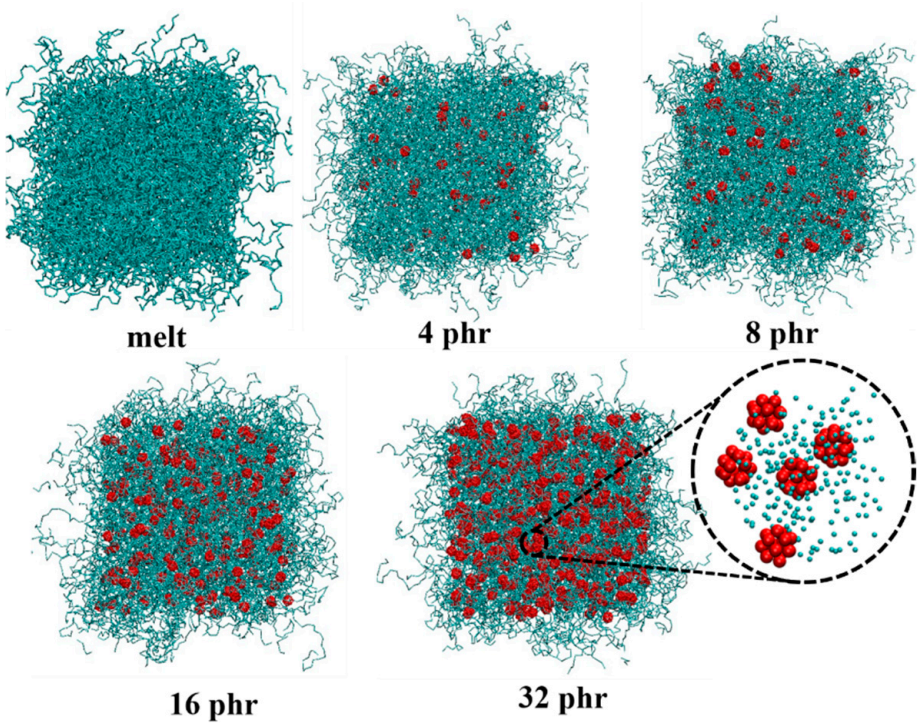

Figure 3. Snapshots of *cis*-PI-C_{60} composites at different C_{60} concentrations from 0 (melt) to 32 phr. Cyan and red represent *cis*-PI and C_{60}, respectively.

In Figure 2a,b, the first and second local minima are at 0.8 nm and 1.2 nm, respectively. Regarding the first local minima in Figure 2a,b, the free energy for C_{60}-*cis*-PI is lower than for C_{60}-C_{60}, indicating a preference for the C_{60}-*cis*-PI interaction. Moreover, in the case of C_{60}-C_{60} interaction, a concentration dependence was observed in which the free energy decreased slowly upon increasing the C_{60} concentration from 4 to 8 phr. For the C_{60}-*cis*-PI, only a minor concentration dependence is present.

3.3.2. Diffusion of C_{60} and *cis*-PI in the Composites

The diffusion coefficients of the C_{60} and *cis*-PI in the melts and in the composites were analyzed at different C_{60} concentrations using the mean squared displacement (MSD)

$$MSD = \left\langle r^2(t) \right\rangle \sim 6Dt \quad (6)$$

where D is the diffusion coefficient and t is time.

In agreement with previous studies [38,87], the presence of C_{60} caused a dramatic decrease in both the C_{60} and *cis*-PI diffusion coefficients (Figure 4). The slow movement at high C_{60} concentration led to confinement, with the C_{60} molecules being more mobile than the *cis*-PI ones. The difference between the diffusion coefficients of C_{60} and *cis*-PI decreased upon increasing the C_{60} concentration; the increased interactions between C_{60} and *cis*-PI cause a reduction in the diffusive motions of C_{60} and *cis*-PI, which is the reason why the bulk modulus of the composites at high C_{60} concentrations becomes enhanced. Note that the diffusion coefficients, extracted from the CG simulations, were one order of magnitude faster than those obtained from the UA simulations [38]. This is due to the reduction of degrees of freedom in the CG model [93].

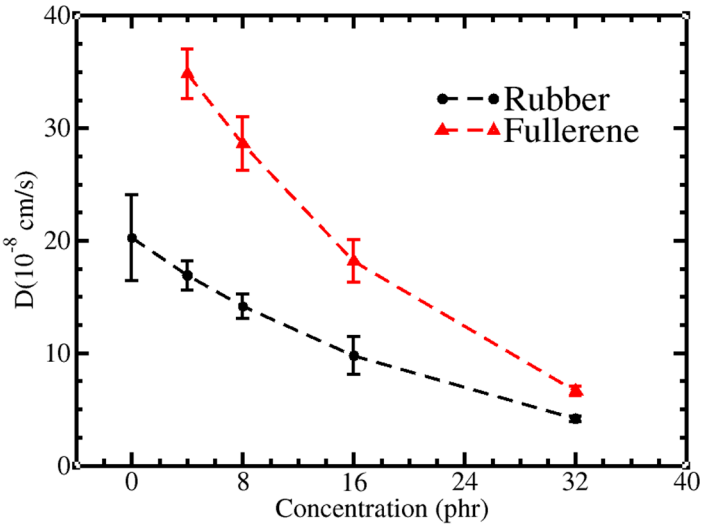

Figure 4. Black line: the diffusion coefficients of rubber in melt (0 phr) and composites (phr $\neq$ 0). Red line: the diffusion coefficients of C_{60} in composites as a function of C_{60} concentration.

3.4. Effect of C_{60} Concentration on C_{60} Solvation Free Energy

The solvation free energies of C_{60} in water, *cis*-PI melt, and *cis*-PI-C_{60} matrix composites were estimated by thermodynamic integration (TI) [78]. The solvation free energy of C_{60} in water was -99.53 ± 0.03 kJ/mol, which is in good agreement with our previous CGMD calculation using umbrella sampling (-92.6 kJ/mol) [94]. Figure 5 shows the concentration dependence of the solvation free energy. The lowest value (~ -115.53 kJ/mol) was found when an added C_{60} was solvated in a *cis*-PI melt. It indicates that the *cis*-PI melt is more favorable than water. Increasing the amount of C_{60} concentration led to lesser solvation in the composites. Our results suggest that the C_{60} prefers to interact with the *cis*-PI chains rather than the other C_{60} molecules in the *cis*-PI-C_{60} composites (Figure 2a,b).

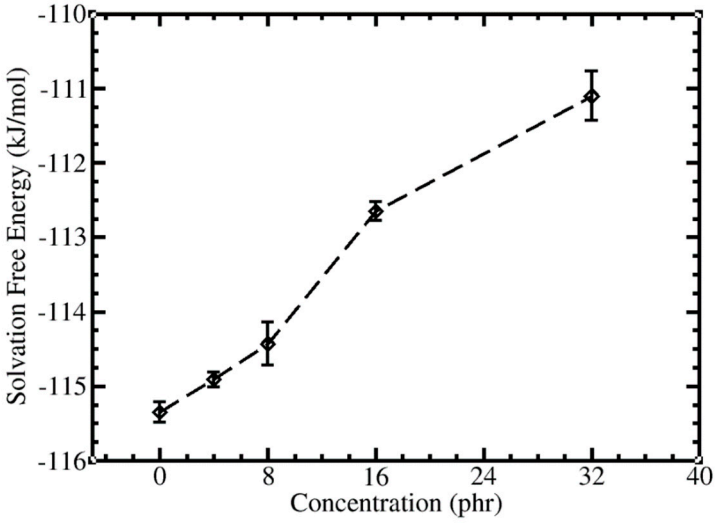

Figure 5. Solvation free energies of C_{60} in *cis*-PI melt (0 phr) and *cis*-PI-C_{60} composites at different C_{60} concentrations. The dashed line is a guide to the eye.

3.5. Effect of C_{60} Concentration on Glass Transition Temperature (T_g)

As discussed above, the CGMD simulations of *cis*-PI-C_{60} composites using our model are able to reproduce the results from previous experiments and atomistic MD simulations [50,95]. The glass transition temperature (T_g) is one of the most important parameters determining the physical state and final mechanical properties of polymer composites [96].

To gain more understanding on the influence of the filler concentration on composites' properties, T_g was estimated using the change of slope in density (ρ) versus temperature (T) curve [75–77]. The ρ-T curves of the *cis*-PI in the melts and composites are shown in Figure S3. The calculated T_g was 201 K, in good agreement with the all-atom (209 K) [77] and united-atom models (223 K) of Sharma et al., [77], and experimental data (200 K) of Brandrup et al. [82] Finally, the concentration dependence of the T_g in the composites was determined. The data in Figure 6 show a linear increase with a slope of 0.63 K/phr. This same trend has been reported in previous experiments [34] and simulations [41,87].

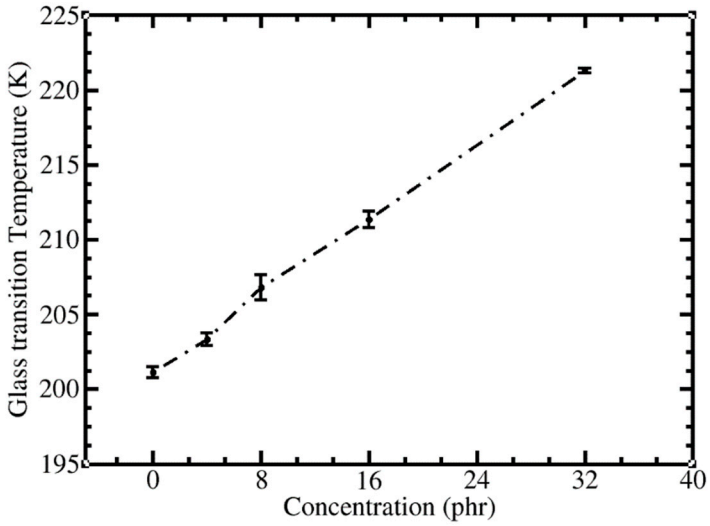

Figure 6. Glass transition temperature (T_g) of *cis*-PI-C_{60} composites at different C_{60} concentrations.

4. Conclusions

We have developed a MARTINI force field version 2.1-based [52] parameterization and performed systematic studies of *cis*-PI in melts and *cis*-PI-C_{60} composites using it. We validated the thermodynamic, macroscopic, and microscopic properties of the *cis*-PI in the melts, and the results show good agreement with prior experimental [80–83] and computational studies [38,77,94]. Perhaps most surprisingly, only a 0.5% difference with respect to the experimentally found glass transition temperature (T_g) [82] in the *cis*-PI in the melts was found.

The properties of the NR-fullerene composites at different C_{60} concentrations (0, 4, 8, 16, and 32 phr) were studied by using CGMD simulations over 200 microseconds. The density, bulk modulus, thermal expansion, heat capacity, and glass transition temperature increased upon increasing the C_{60} concentration. A slight increase in the R_0 and R_g of the *cis*-PI chains was found for the NR-C_{60} composites. The interaction energies between the C_{60} and *cis*-PI decreased when the amount of C_{60} increased. The diffusion of the *cis*-PI and C_{60} was slowed down by increasing the C_{60} concentration. The decrease of the interaction free energies and the diffusion coefficients resulted in an enhancement of the bulk modulus of the composites. Moreover, the solvation free energies of the C_{60} in the *cis*-PI matrix composites increased upon increasing the C_{60} concentration. These results suggest that C_{60}-*cis*-PI interactions are more preferable than C_{60}-C_{60} self-interactions.

The CG model introduced here allows simulations of large systems over long periods of time to study properties such as the impact of the filler concentration on rubber composites at the molecular level. This validated *cis*-PI-C_{60} CG model based on the MARTINI force field will also enable simulations of the advanced rubber materials and their interactions with biological molecules.

Supplementary Materials: The following are available online at https://www.mdpi.com/article/10.3390/polym13224044/s1, Table S1: Details of the CG force field for cis-PI, Table S2: Number of molecules and simulation time, Table S3: Solvation free energy of an added fullerene in water, cis-PI in melt and composite at different C60 concentrations, Figure S1: Time evolution of end-to-end distance (R0) with varies C60 concentration from 0 to 32 phr, Figure S2: Time evolution of radius of gyration (Rg) with varies C60 concentration from 0 to 32 phr, Figure S3: Density versus temperature of cis-PI-C60 composites.

Author Contributions: Conceptualization, J.W.-e; methodology, J.K. and J.W.-e.; software, J.K., T.S. and J.W.-e.; validation, J.K., W.K. and J.W.-e.; formal analysis, J.K.; investigation, J.K., W.K. and J.W.-e.; resources, J.W.-e.; data curation, J.K., W.K.; writing—original draft preparation, J.K., W.K. and J.W.-e.; writing—review and editing, J.W.-e., M.K., S.P., T.S., and N.C.; visualization, J.K.; supervision, J.W.-e. and M.K.; project administration, J.W.-e.; funding acquisition, J.W.-e. and N.C. All authors have read and agreed to the published version of the manuscript.

Funding: This research was funded by the National Research Council of Thailand (NRCT), Thailand Science Research and Innovation (TSRI), the Kasetsart University Research and Development Institute (KURDI) and the Faculty of Science, Kasetsart University through the Research Grants for Talented Mid-Career Researchers Grant No. N41A640080, the Royal Golden Jubilee Ph.D. Program Grant No. PHD/0134/2561, and the International Frontier Research Network (IFRN) research fund. The APC was funded by the Royal Golden Jubilee Ph.D. Program Grant No. PHD/0134/2561.

Institutional Review Board Statement: Not applicable.

Informed Consent Statement: Not applicable.

Data Availability Statement: The data presented in this study are available on request from the corresponding author.

Acknowledgments: This work was financially supported by the National Research Council of Thailand (NRCT), Thailand Science Research and Innovation (TSRI) through the Research Grants for Talented Mid-Career Researchers Grant No. N41A640080, and the Royal Golden Jubilee Ph.D. Program Grant No. PHD/0134/2561 (J.W.-e. and J.K.). J.W.-e., N.C., and W.K. acknowledged the Kasetsart University Research and Development Institute (KURDI) and the Faculty of Science, Kasetsart University for supporting the post-doctoral scholarship and the International Frontier Research Network (IFRN) research fund. M.K. thanks the Natural Sciences and Engineering Research Council of Canada (NSERC) and the Canada Research Chairs Program for financial support. Computing facilities were provided by SHARCNET (www.sharcnet.ca, accessed on 22 November 2021), Compute Canada (www.computecanada.ca, accessed on 22 November 2021), and the Department of Physics, Faculty of Science, Kasetsart University.

Conflicts of Interest: The authors declare no competing interest.

References

1. Park, C.Y. Cure characteristics and dynamic mechanical properties of acrylic rubber and epoxidized natural rubber blend. *J. Ind. Eng. Chem.* **2001**, *7*, 212–217.
2. Chollakup, R.; Suethao, S.; Suwanruji, P.; Boonyarit, J.; Smitthipong, W. Mechanical properties and dissipation energy of carbon black/rubber composites. *Compos. Adv. Mater.* **2021**, *30*, 1–6. [CrossRef]
3. Ray, S.S.; Okamoto, M. Polymer/layered silicate nanocomposites: A review from preparation to processing. *Prog. Polym. Sci.* **2003**, *28*, 1539–1641.
4. Moniruzzaman, M.; Winey, K.I. Polymer nanocomposites containing carbon nanotubes. *Macromolecules* **2006**, *39*, 5194–5205. [CrossRef]
5. Caseri, W. Nanocomposites of polymers and metals or semiconductors: Historical background and optical properties. *Macromol. Rapid Commun.* **2000**, *21*, 705–722. [CrossRef]
6. Xie, X.-L.; Mai, Y.-W.; Zhou, X.-P. Dispersion and alignment of carbon nanotubes in polymer matrix: A review. *Mater. Sci. Eng. R Rep.* **2005**, *49*, 89–112. [CrossRef]
7. Balazs, A.C.; Emrick, T.; Russell, T.P. Nanoparticle polymer composites: Where two small worlds meet. *Science* **2006**, *314*, 1107–1110. [CrossRef]
8. Tee, B.C.K.; Wang, C.; Allen, R.; Bao, Z. An Electrically and Mechanically Self-Healing Composite with Pressure- and Flexion-Sensitive Properties for Electronic Skin Applications. *Nat. Nanotechnol.* **2012**, *7*, 825–832. [CrossRef] [PubMed]
9. Du, F.; Scogna, R.C.; Zhou, W.; Brand, S.; Fischer, J.E.; Winey, K.I. Nanotube networks in polymer nanocomposites: Rheology and electrical conductivity. *Macromolecules* **2004**, *37*, 9048–9055. [CrossRef]

10. Oh, H.; Green, P.F. Polymer chain dynamics and glass transition in athermal polymer/nanoparticle mixtures. *Nat. Mater.* **2009**, *8*, 139–143. [CrossRef] [PubMed]
11. Rittigstein, P.; Priestley, R.D.; Broadbelt, L.J.; Torkelson, J.M. Model polymer nanocomposites provide an understanding of confinement effects in real nanocomposites. *Nat. Mater.* **2007**, *6*, 278–282. [CrossRef]
12. Suethao, S.; Phongphanphanee, S.; Wong-Ekkabut, J.; Smitthipong, W. The Relationship between the Morphology and Elasticity of Natural Rubber Foam Based on the Concentration of the Chemical Blowing Agent. *Polymers* **2021**, *13*, 1091. [CrossRef]
13. Suethao, S.; Ponloa, W.; Phongphanphanee, S.; Wong-Ekkabut, J.; Smitthipong, W. Current challenges in thermodynamic aspects of rubber foam. *Sci. Rep.* **2021**, *11*, 1–12.
14. Wichaita, W.; Promlok, D.; Sudjaipraparat, N.; Sripraphot, S.; Suteewong, T.; Tangboriboonrat, P. A Concise Review on Design and Control of Structured Natural Rubber Latex Particles as Engineering Nanocomposites. *Eur. Polym. J.* **2021**, *159*, 110740. [CrossRef]
15. Calabrese, M.A.; Chan, W.Y.; Av-Ron, S.H.; Olsen, B.D. Development of a Rubber Recycling Process Based on a Single-Component Interfacial Adhesive. *ACS Appl. Polym. Mater.* **2021**, *3*, 4849–4860. [CrossRef]
16. Gielen, D.; Bennaceur, K.; Kerr, T.; Tam, C.; Tanaka, K.; Taylor, M.; Taylor, P. *Tracking Industrial Energy Efficiency and CO_2 Emissions*; International Energy Agency: Paris, France, 2007.
17. Phuhiangpa, N.; Ponloa, W.; Phongphanphanee, S.; Smitthipong, W. Performance of nano- and microcalcium carbonate in uncrosslinked natural rubber composites: New results of structure–properties relationship. *Polymers* **2020**, *12*, 2002. [CrossRef]
18. Maiti, M.; Sadhu, S.; Bhowmick, A.K. Effect of carbon black on properties of rubber nanocomposites. *J. Appl. Polym. Sci.* **2005**, *96*, 443–451. [CrossRef]
19. Araby, S.; Meng, Q.; Zhang, L.; Zaman, I.; Majewski, P.; Ma, J. Elastomeric composites based on carbon nanomaterials. *Nanotechnology* **2015**, *26*, 112001. [CrossRef] [PubMed]
20. Sisanth, K.; Thomas, M.; Abraham, J.; Thomas, S. General introduction to rubber compounding. In *Progress in Rubber Nanocomposites*; Thomas, S., Maria, H.J., Eds.; Elsevier: Amsterdam, The Netherlands, 2017; pp. 1–39.
21. Zhang, H.; Zhang, Z.; Zhao, G.; Liu, Y. Influence of carbon black with different concentration on dynamic properties and heat buildup of semi-efficient natural rubber composites. *Micro Nano Lett.* **2016**, *11*, 402–406. [CrossRef]
22. Savetlana, S.; Zulhendri; Sukmana, I.; Saputra, F. The effect of carbon black loading and structure on tensile property of natural rubber composite. *IOP Conf. Ser. Mater. Sci. Eng.* **2017**, *223*, 012009. [CrossRef]
23. Luheng, W.; Tianhuai, D.; Peng, W. Influence of carbon black concentration on piezoresistivity for carbon-black-filled silicone rubber composite. *Carbon* **2009**, *47*, 3151–3157. [CrossRef]
24. Scagliusi, S.R.; Cardoso, E.C.L.; Parra, D.F.; Lima, L.F.C.P.; Lugão, A.B. Evaluation of "Payne effect" in radiation-induced modification of chlorobutyl rubber. *Radiat. Phys. Chem.* **2013**, *84*, 42–46. [CrossRef]
25. Payne, A.R. The dynamic properties of carbon black-loaded natural rubber vulcanizates. Part I. *J. Appl. Polym. Sci.* **1962**, *6*, 57–63. [CrossRef]
26. United States Environmental Protection Agency. *Compilation of Air Pollutant Emission Factors*, 5th ed.; Office of Air Quality Planning and Standards: Durham, NC, USA, 1995.
27. Yang, M.; Koutsos, V.; Zaiser, M. Interactions between polymers and carbon nanotubes: A molecular dynamics study. *J. Phys. Chem. B* **2005**, *109*, 10009–10014. [CrossRef]
28. Dresselhaus, M.S.; Dresselhaus, G.; Eklund, P.C. *Science of Fullerenes and Carbon Nanotubes: Their Properties and Applications*; Elsevier: Amsterdam, The Netherlands, 1996.
29. George, N.; Chandra, J.; Mathiazhagan, A.; Joseph, R. High performance natural rubber composites with conductive segregated network of multiwalled carbon nanotubes. *Compos. Sci. Technol.* **2015**, *116*, 33–40. [CrossRef]
30. Chirvase, D.; Parisi, J.; Hummelen, J.C.; Dyakonov, V. Influence of nanomorphology on the photovoltaic action of polymer–fullerene composites. *Nanotechnology* **2004**, *15*, 1317–1323. [CrossRef]
31. Thompson, B.C.; Fréchet, J.M.J. Polymer-fullerene composite solar cells. *Angew. Chem. Int. Ed.* **2008**, *47*, 58–77. [CrossRef]
32. Dennler, G.; Scharber, M.C.; Brabec, C.J. Polymer-fullerene bulk-heterojunction solar cells. *Adv. Mater.* **2009**, *21*, 1323–1338. [CrossRef]
33. Kausar, A. Fullerene nanofiller reinforced epoxy nanocomposites—Developments, progress and challenges. *Mater. Res. Innov.* **2020**, *25*, 175–185. [CrossRef]
34. Al-Hartomy, O.A.; Al-Ghamdi, A.A.; Al-Salamy, F.; Dishovsky, N.; Slavcheva, D.; El-Tantawy, F. Properties of natural rubber-based composites containing fullerene. *Int. J. Polym. Sci.* **2012**, *2012*, 967276. [CrossRef]
35. Jurkowska, B.; Jurkowski, B.; Kamrowski, P.; Pesetskii, S.S.; Koval, V.N.; Pinchuk, L.S.; Olkhov, Y.A. Properties of fullerene-containing natural rubber. *J. Appl. Polym. Sci.* **2006**, *100*, 390–398. [CrossRef]
36. Liu, J.; Gao, Y.; Cao, D.; Zhang, L.; Guo, Z. Nanoparticle dispersion and aggregation in polymer nanocomposites: Insights from molecular dynamics simulation. *Langmuir* **2011**, *27*, 7926–7933. [CrossRef]
37. Guseva, D.V.; Komarov, P.V.; Lyulin, A.V. Molecular-dynamics simulations of thin polyisoprene films confined between amorphous silica substrates. *J. Chem. Phys.* **2014**, *140*, 114903. [CrossRef]
38. Khuntawee, W.; Sutthibutpong, T.; Phongphanphanee, S.; Karttunen, M.; Wong-Ekkabut, J. Molecular dynamics study of natural rubber-fullerene composites: Connecting microscopic properties to macroscopic behavior. *Phys. Chem. Chem. Phys.* **2019**, *21*, 19403–19413. [CrossRef]

39. Ghanbari, A.; Rahimi, M.; Dehghany, J. Influence of surface grafted polymers on the polymer dynamics in a silica-polystyrene nanocomposite: A coarse-grained molecular dynamics investigation. *J. Phys. Chem. C* **2013**, *117*, 25069–25076. [CrossRef]
40. Davris, T.; Mermet-Guyennet, M.R.B.; Bonn, D.; Lyulin, A.V. Filler size effects on reinforcement in elastomer-based nanocomposites: Experimental and simulational insights into physical mechanisms. *Macromolecules* **2016**, *49*, 7077–7087. [CrossRef]
41. Liu, J.; Wu, Y.; Shen, J.; Gao, Y.; Zhang, L.; Cao, D. Polymer–nanoparticle interfacial behavior revisited: A molecular dynamics study. *Phys. Chem. Chem. Phys.* **2011**, *13*, 13058–13069. [CrossRef] [PubMed]
42. Raffaini, G.; Citterio, A.; Galimberti, M.; Catauro, M. A Molecular dynamics study of noncovalent interactions between rubber and fullerenes. *Macromol. Symp.* **2021**, *395*, 2000198. [CrossRef]
43. Kremer, K.; Grest, G.S. Dynamics of entangled linear polymer melts: A molecular-dynamics simulation. *J. Chem. Phys.* **1990**, *92*, 5057–5086. [CrossRef]
44. Forrest, B.M.; Suter, U.W. Accelerated equilibration of polymer melts by time-coarse-graining. *J. Chem. Phys.* **1995**, *102*, 7256–7266. [CrossRef]
45. Akkermans, R.L.C.; Briels, W.J. A structure-based coarse-grained model for polymer melts. *J. Chem. Phys.* **2001**, *114*, 1020–1031. [CrossRef]
46. Faller, R. Automatic coarse graining of polymers. *Polymer* **2004**, *45*, 3869–3876. [CrossRef]
47. Reith, D.; Meyer, H.; Müller-Plathe, F. Mapping atomistic to coarse-grained polymer models using automatic simplex optimization to fit structural properties. *Macromolecules* **2001**, *34*, 2335–2345. [CrossRef]
48. Nikunen, P.; Vattulainen, I.; Karttunen, M. Reptational dynamics in dissipative particle dynamics simulations of polymer melts. *Phys. Rev. E* **2007**, *75*, 036713. [CrossRef]
49. Vettorel, T.; Besold, G.; Kremer, K. Fluctuating soft-sphere approach to coarse-graining of polymer models. *Soft Matter* **2010**, *6*, 2282–2292. [CrossRef]
50. Huang, D.M.; Faller, R.; Do, K.; Moulé, A.J. Coarse-grained computer simulations of polymer/fullerene bulk heterojunctions for organic photovoltaic applications. *J. Chem. Theory Comput.* **2010**, *6*, 526–537. [CrossRef]
51. Volgin, I.V.; Larin, S.V.; Lyulin, A.V.; Lyulin, S.V. Coarse-grained molecular-dynamics simulations of nanoparticle diffusion in polymer nanocomposites. *Polymer* **2018**, *145*, 80–87. [CrossRef]
52. Marrink, S.J.; Risselada, H.J.; Yefimov, S.; Tieleman, D.P.; de Vries, A.H. The MARTINI force field: Coarse grained model for biomolecular simulations. *J. Phys. Chem. B* **2007**, *111*, 7812–7824. [CrossRef]
53. Marrink, S.J.; Tieleman, D.P. Perspective on the Martini model. *Chem. Soc. Rev.* **2013**, *42*, 6801–6822. [CrossRef] [PubMed]
54. Monticelli, L.; Kandasamy, S.K.; Periole, X.; Larson, R.G.; Tieleman, D.P.; Marrink, S.J. The MARTINI coarse-grained force field: Extension to proteins. *J. Chem. Theory Comput.* **2008**, *4*, 819–834. [CrossRef]
55. Marrink, S.J.; de Vries, A.H.; Mark, A.E. Coarse grained model for semiquantitative lipid simulations. *J. Phys. Chem. B* **2004**, *108*, 750–760. [CrossRef]
56. Wong-Ekkabut, J.; Baoukina, S.; Triampo, W.; Tang, I.-M.; Tieleman, D.P.; Monticelli, L. Computer simulation study of fullerene translocation through lipid membranes. *Nat. Nanotechnol.* **2008**, *3*, 363. [CrossRef]
57. Rossi, G.; Monticelli, L.; Puisto, S.R.; Vattulainen, I.; Ala-Nissila, T. Coarse-graining polymers with the MARTINI force-field: Polystyrene as a benchmark case. *Soft Matter* **2011**, *7*, 698–708. [CrossRef]
58. Uusitalo, J.J.; Ingólfsson, H.I.; Marrink, S.J.; Faustino, I. Martini coarse-grained force field: Extension to RNA. *Biophys. J.* **2017**, *113*, 246–256. [CrossRef]
59. Nisoh, N.; Jarerattanachat, V.; Karttunen, M.; Wong-Ekkabut, J. Formation of aggregates, icosahedral structures and percolation clusters of fullerenes in lipids bilayers: The key role of lipid saturation. *Biochim. Biophys. Acta Biomembr.* **2020**, *1862*, 183328. [CrossRef]
60. Nalakarn, P.; Boonnoy, P.; Nisoh, N.; Karttunen, M.; Wong-Ekkabut, J. Dependence of fullerene aggregation on lipid saturation due to a balance between entropy and enthalpy. *Sci. Rep.* **2019**, *9*, 1037. [CrossRef] [PubMed]
61. Ingólfsson, H.I.; Melo, M.N.; van Eerden, F.J.; Arnarez, C.; Lopez, C.A.; Wassenaar, T.A.; Periole, X.; de Vries, A.H.; Tieleman, D.P.; Marrink, S.J. Lipid organization of the plasma membrane. *J. Am. Chem. Soc.* **2014**, *136*, 14554–14559. [CrossRef] [PubMed]
62. Kitjanon, J.; Khuntawee, W.; Sutthibutpong, T.; Boonnoy, P.; Phongphanphanee, S.; Wong-ekkabut, J. Transferability of Polymer Chain Properties between Coarse-Grained and Atomistic Models of Natural Rubber Molecule Validated by Molecular Dynamics Simulations. *J. Phys. Conf. Ser.* **2017**, *901*, 012096. [CrossRef]
63. Monticelli, L. On atomistic and coarse-grained models for C60 fullerene. *J. Chem. Theory Comput.* **2012**, *8*, 1370–1378. [CrossRef]
64. Abraham, M.J.; Murtola, T.; Schulz, R.; Páll, S.; Smith, J.C.; Hess, B.; Lindahl, E. GROMACS: High performance molecular simulations through multi-level parallelism from laptops to supercomputers. *SoftwareX* **2015**, *1–2*, 19–25. [CrossRef]
65. Bussi, G.; Donadio, D.; Parrinello, M. Canonical sampling through velocity rescaling. *J. Chem. Phys.* **2007**, *126*, 014101. [CrossRef]
66. Bussi, G.; Zykova-Timan, T.; Parrinello, M. Isothermal-isobaric molecular dynamics using stochastic velocity rescaling. *J. Chem. Phys.* **2009**, *130*, 074101. [CrossRef] [PubMed]
67. Parrinello, M.; Rahman, A. Polymorphic transitions in single crystals: A new molecular dynamics method. *J. Appl. Phys.* **1981**, *52*, 7182–7190. [CrossRef]
68. Wassenaar, T.A.; Ingólfsson, H.I.; Prieß, M.; Marrink, S.J.; Schäfer, L.V. Mixing MARTINI: Electrostatic coupling in hybrid atomistic-coarse-grained biomolecular simulations. *J. Phys. Chem. B* **2013**, *117*, 3516–3530. [CrossRef]

69. Beu, T.A.; Ailenei, A.E.; Costinaş, R.I. Martini Force Field for Protonated Polyethyleneimine. *J. Comput. Chem.* **2020**, *41*, 349–361. [CrossRef] [PubMed]
70. Wong-Ekkabut, J.; Karttunen, M. The good, the bad and the user in soft matter simulations. *Biochim. Biophys. Acta Biomembr.* **2016**, *1858*, 2529–2538. [CrossRef]
71. Wong-Ekkabut, J.; Karttunen, M. Molecular dynamics simulation of water permeation through the alpha-hemolysin channel. *J. Biol. Phys.* **2016**, *42*, 133–146. [CrossRef] [PubMed]
72. Boonnoy, P.; Karttunen, M.; Wong-Ekkabut, J. Does α-tocopherol flip-flop help to protect membranes against oxidation? *J. Phys. Chem. B* **2018**, *122*, 10362–10370. [CrossRef] [PubMed]
73. Enkavi, G.; Javanainen, M.; Kulig, W.; Róg, T.; Vattulainen, I. Multiscale simulations of biological membranes: The challenge to understand biological phenomena in a living substance. *Chem. Rev.* **2019**, *119*, 5607–5774. [CrossRef] [PubMed]
74. Humphrey, W.; Dalke, A.; Schulten, K. VMD: Visual molecular dynamics. *J. Mol. Graph.* **1996**, *14*, 33–38. [CrossRef]
75. Buchholz, J.; Paul, W.; Varnik, F.; Binder, K. Cooling rate dependence of the glass transition temperature of polymer melts: Molecular dynamics study. *J. Chem. Phys.* **2002**, *117*, 7364–7372. [CrossRef]
76. Glova, A.D.; Falkovich, S.G.; Dmitrienko, D.I.; Lyulin, A.V.; Larin, S.V.; Nazarychev, V.M.; Karttunen, M.; Lyulin, S.V. Scale-dependent miscibility of polylactide and polyhydroxybutyrate: Molecular dynamics simulations. *Macromolecules* **2018**, *51*, 552–563. [CrossRef]
77. Sharma, P.; Roy, S.; Karimi-Varzaneh, H.A. Validation of force fields of rubber through glass-transition temperature calculation by microsecond atomic-scale molecular dynamics simulation. *J. Phys. Chem. B* **2016**, *120*, 1367–1379. [CrossRef]
78. Van Gunsteren, W.F.; Weiner, P.K.; Wilkinson, A.J. *Computer Simulation of Biomolecular Systems: Theoretical and Experimental Applications*; Springer Science & Business Media: Berlin, Germany, 2013; Volume 3.
79. Bennett, C.H. Efficient estimation of free energy differences from Monte Carlo data. *J. Comput. Phys.* **1976**, *22*, 245–268. [CrossRef]
80. Fetters, L.J.; Lohse, D.J.; Graessley, W.W. Chain dimensions and entanglement spacings in dense macromolecular systems. *J. Polym. Sci. Part B Polym. Phys.* **1999**, *37*, 1023–1033. [CrossRef]
81. Tobolsky, A.V.; Mark, H.F. *Polymer Science and Materials*; John Wiley and Sons: Hoboken, NJ, USA, 1971.
82. Brandrup, J.; Immergut, E.H.; Grulke, E.A.; Abe, A.; Bloch, D.R. *Polymer Handbook*; John Wiley and Sons: Hoboken, NJ, USA, 1999.
83. Holownia, B.P. Effect of carbon black on Poisson's ratio of elastomers. *Rubber Chem. Technol.* **1975**, *48*, 246–253. [CrossRef]
84. Guenza, M. Structural and thermodynamic consistency in coarse-grained models of macromolecules. *J. Phys. Conf. Ser.* **2015**, *640*, 012009. [CrossRef]
85. Potestio, R.; Peter, C.; Kremer, K. Computer simulations of soft matter: Linking the scales. *Entropy* **2014**, *16*, 4199–4245. [CrossRef]
86. Van der Wal, C.W.; Bree, H.W.; Schwarzl, F.R. Mechanical properties of highly filled elastomers. II. Relationship between filler characteristics, thermal expansion, and bulk moduli. *J. Appl. Polym. Sci.* **1965**, *9*, 2143–2166. [CrossRef]
87. Wei, C.; Srivastava, D.; Cho, K. Thermal expansion and diffusion coefficients of carbon nanotube-polymer composites. *Nano Lett.* **2002**, *2*, 647–650. [CrossRef]
88. Wang, S.; Tambraparni, M.; Qiu, J.; Tipton, J.; Dean, D. Thermal expansion of graphene composites. *Macromolecules* **2009**, *42*, 5251–5255. [CrossRef]
89. Vettorel, T.; Kremer, K. Development of entanglements in a fully disentangled polymer melt. *Macromol. Theory Simul.* **2010**, *19*, 44–56. [CrossRef]
90. Mcquarrie, D. *Statistical Mechanics*; Harper & Row: New York, NY, USA, 1976.
91. Trzesniak, D.; Kunz, A.P.E.; van Gunsteren, W.F. A comparison of methods to compute the potential of mean force. *Chemphyschem* **2007**, *8*, 162–169. [CrossRef] [PubMed]
92. Cao, Z.; Peng, Y.; Li, S.; Liu, L.; Yan, T. Molecular dynamics simulation of fullerene C60 in ethanol solution. *J. Phys. Chem. C* **2009**, *113*, 3096–3104. [CrossRef]
93. Al-Qattan, M.N.; Deb, P.K.; Tekade, R.K. Molecular dynamics simulation strategies for designing carbon-nanotube-based targeted drug delivery. *Drug Discov. Today* **2018**, *23*, 235–250. [CrossRef]
94. Nisoh, N.; Karttunen, M.; Monticelli, L.; Wong-Ekkabut, J. Lipid monolayer disruption caused by aggregated carbon nanoparticles. *RSC Adv.* **2015**, *5*, 11676–11685. [CrossRef]
95. Chakrabarty, A.; Cagin, T. Coarse grain modeling of polyimide copolymers. *Polymer* **2010**, *51*, 2786–2794. [CrossRef]
96. Sillescu, H. Heterogeneity at the glass transition: A review. *J. Non -Cryst. Solids* **1999**, *243*, 81–108. [CrossRef]